Computational Modeling of Interfacial Debonding in Fused Silica/AA7020 Alloy Particle-Reinforced Metal Matrix Composites

[1]H. B. Nirnajan and A. Chennakesava Reddy[2]

[1]Associate Professor, Department of Mechanical Engineering, M. S. Ramaiah Institute of Technology, Bangalore, India.
[2]Associate Professor, Department of Mechanical Engineering, Vasavi College of Engineering, Hyderabad, India
dr_acreddy@yahoo.com

Abstract: *A diamond array unit cell/rhombus SiO_2 nanoparticle RVE models were used to predict micromechanical behavior and interfacial debonding in AA7020/* SiO_2 *composites. The AA7020/* SiO_2 *metal matrix composites were fabricated at 10%, 20% and 30% volume fractions of SiO2. The microstructure of AA7020 alloy/ SiO_2 reveals the presence of porosity, interfacial debonding and matrix fracture.*

Keywords: AA7020*, fused silica, rhombus nanoparticle, RVE model, finite element analysis, debonding.*

1. INTRODUCTION

Adhesion between particle and matrix is controlled by properties of the interface in the particle reinforced metal matrix composites. Generally high degree of adhesion is desirable to provide efficient of transfer of load between particle and matrix. Many factors responsible for the macroscopic properties of the composites are discussed in the literature, including load transfer between the matrix and reinforcements [1], presence of precipitations at the matrix/particle interface, mechanical characteristics of individual components of the materials [2], residual stresses resulting from the technological processing of a mismatch between the thermal expansion coefficients of the components [3]. Important characteristics providing a key contribution to damage accumulation and fracture of the materials are the reinforcing particle size, shape, volume fraction, and spatial distribution [4]. The interfacial reinforcement reflects the progressed fracture rather than the instantaneous fracture. In a series of research, a variety of nanoparticle shapes such as spherical [5, 6], ellipsoidal [7-11], rectangular [12], hexagonal [13-15] and rhombus [16] at 10%, 20% and 30% volume fractions were studied and the results computed from a unit cell with uniformly distributed particles were compared.

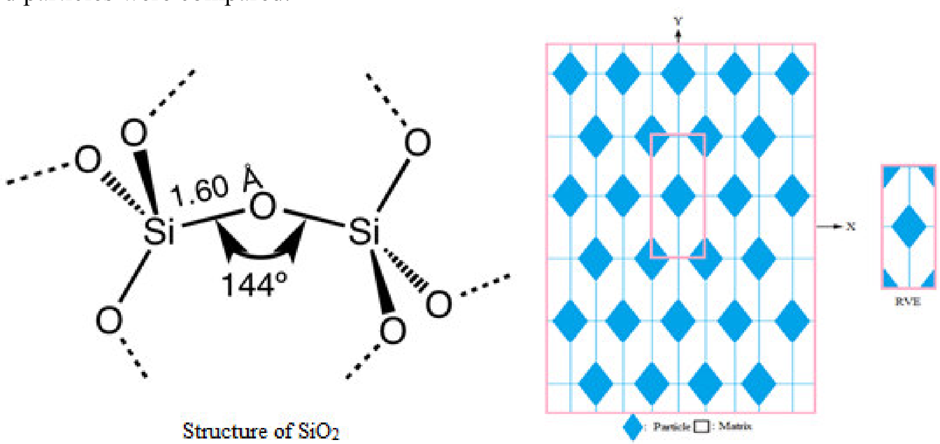

Figure 1: A hexagonal RVE containing an ellipsoidal nanoparticle.

Silica is one of the most complex and most abundant families of materials, existing both as several minerals and being produced synthetically. Notable examples include fused quartz, crystal, fumed silica, silica gel, and aerogels. Silicon dioxide is mostly obtained by mining and purification of quartz. In the majority of silicates, the Si atom shows tetrahedral coordination, with 4 oxygen atoms surrounding a central Si atom. The most common example is seen in the quartz crystalline form of silica SiO_2. In each of the most thermodynamically stable crystalline forms of silica, on average, all 4 of the vertices (or oxygen atoms) of the SiO_4 tetrahedra are shared with others, yielding the net chemical formula: SiO_2 (figure 1). In the present work, zirconia nanoparticles were reinforced in AA7020 alloy through the stir casting process. The effect of varying volume fractions of SiO_2 on the microstructural and mechanical properties of AA7020 alloy is examined. The structure-property relationship is used to understand the observed mechanical behavior of the developed AA7020 alloy/ SiO_2 composites. The shape of SiO_2 nanoparticle considered in this work is a hexagonal. The periodic particle distribution was a hexagonal array as shown in figure 1.

2. THEORETICAL BACKGROUND

The strains along x- and y-directions can be determined as using the following equations:

$$\varepsilon_y = -\left(\frac{v_{xy}}{E_x} + \frac{1}{E_z}\right) P = \frac{\Delta y}{a} \quad (1)$$

$$\varepsilon_x = \left(\frac{1}{E_x} - \frac{1}{E_z}\right) P = \frac{\Delta x}{a} \quad (2)$$

The effective elastic moduli and Poisson's ratio in the transverse direction (xy-plane) as follows:

$$E_x = \frac{1}{\frac{\Delta x}{Pa} + \frac{1}{E_z}} \text{ and } E_y = \frac{1}{\frac{\Delta y}{Pa} + \frac{1}{E_z}} \quad (3)$$

$$v_{xy} = \left(\frac{\Delta y}{Pa} + \frac{1}{E_z}\right) / \left(\frac{\Delta x}{Pa} + \frac{1}{E_z}\right) \quad (4)$$

Once the change in lengths along x- and y- direction (Δx and Δy) are determined for the square RVE from the FEA, E_y and E_x and v_{xy} can be determined from Eqs. (3) and (4), correspondingly. Considering adhesion, formation of precipitates, particle size, agglomeration, voids/porosity, obstacles to the dislocation, and the interfacial reaction of the particle/matrix, the formula for the strength of composite is stated below:

$$\sigma_c = \left[\sigma_m \left\{\frac{1-(v_p+v_v)^{2/3}}{1-1.5(v_p+v_v)}\right\}\right] e^{m_p(v_p+v_v)} + k d_p^{-1/2} \quad (5)$$

$$k = E_m m_m / E_p m_p$$

where, v_v and v_p are the volume fractions of voids/porosity and nanoparticles in the composite respectively, m_p and m_m are the possion's ratios of the nanoparticles and matrix respectively, d_p is the mean nanoparticle size (diameter) and E_m and E_p is elastic moduli of the matrix and the particle respectively. Elastic modulus (Young's modulus) is a measure of the stiffness of a material and is a quantity used to characterize materials. Elastic modulus is the same in all orientations for isotropic materials. Anisotropy can be seen in many composites.

The upper-bound equation is given by

$$\frac{E_c}{E_m} = \left(\frac{1-v_v^{2/3}}{1-v_v^{2/3}+v_v}\right) + \frac{1+(\delta-1)v_p^{2/3}}{1+(\delta-1)(v_p^{2/3}-v_p)} \quad (6)$$

The lower-bound equation is given by

$$\frac{E_c}{E_m} = 1 + \frac{v_p - v_p}{\delta/(\delta-1)-(v_p+v_v)^{1/3}} \quad (7)$$

where, $\delta = E_p / E_m$.

The transverse modulus is given by

$$E_t = \frac{E_m E_p}{E_m + E_p(1-v_p^{2/3})/v_p^{2/3}} + E_m\left(1 - v_p^{2/3} - v_v^{2/3}\right) \quad (8)$$

3. MATERIALS METHODS

The matrix material was AA7020 alloy. The reinforcement material was ellipsoidal SiO_2 nanoparticles of average size 100nm. The mechanical properties of materials used in the present work are given in table 1.

Table 1: Mechanical properties of AA7020 matrix and SiO_2 nanoparticles

Property	AA7020	SiO_2
Density, g/cc	2.78	2.20
Elastic modulus, GPa	72.0	73.1
Ultimate tensile strength, MPa	350	110
Poisson's ratio	0.33	0.17

AA7020 alloy/ SiO_2 composites were manufactured by the stir casting process and low pressure casting technique with argon gas at 3.0 bar. The composite samples were give solution treatment and cold rolled to the predefined size of tensile specimens. The heat-treated samples were machined to get flat-rectangular specimens (figure 2) for the tensile tests. The tensile specimens were placed in the grips of a Universal Test Machine (UTM) at a specified grip separation and pulled until failure. The test speed was 2 mm/min. A strain gauge was used to determine elongation. In this research, a cubical representative volume element (RVE) was implemented to analyze the tensile behavior AA7020/ SiO_2 nanoparticle composites at three (10%, 20% and 30%) volume fractions of SiO_2. The large strain PLANE183 element was used in the matrix in all the models. In order to model the adhesion between the matrix and the particle, a CONTACT 172 element was used.

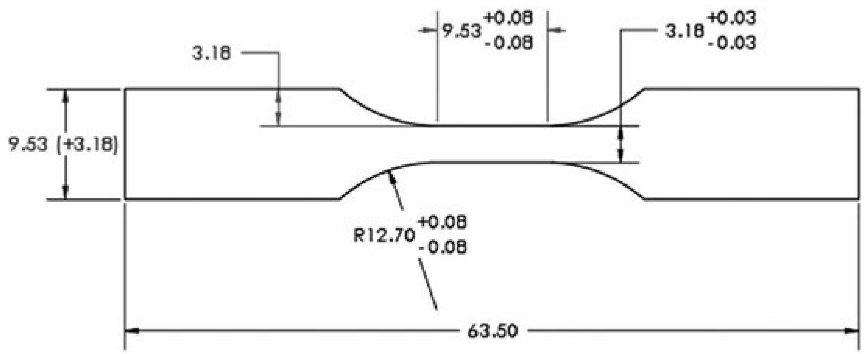

Figure 2: Shape and dimensions of tensile specimen

4. RESULTS AND DISCUSSION

The micrograph as shown in figure 3 reveals uniform distribution of SiO_2 particles in AA7020 alloy matrix. The tested tensile specimens are shown in figure 4. The necking was formed only the composites having 10% SiO_2. The elongation of was decreased with increased volume fraction of SIO_2 particles in AA7020 alloy matrix.

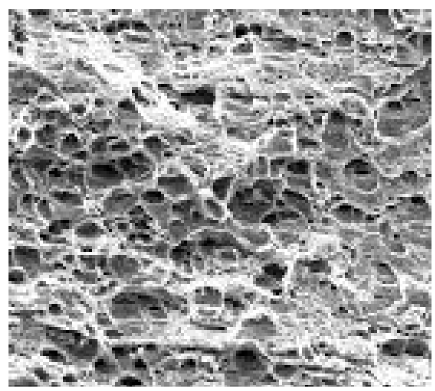

Figure 3: Optical micrograph showing uniform distribution of SiO_2 nanoparticles.

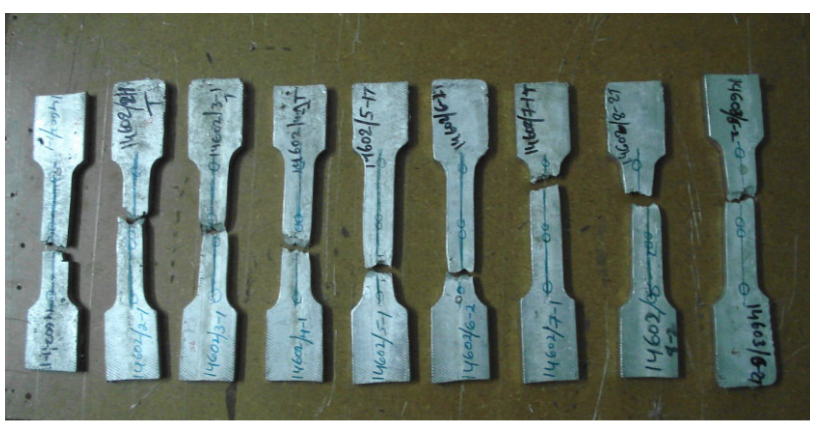

Figure 4: Tested tensile specimens.

4.1 Micromechanical Behavior

Figure 5a represents the normalized tensile strengths of the AA7020 alloy/ SiO_2 composites obtained by FEA, present mathematical model, and experimental test. The tensile strength is normalized with ultimate tensile strength of AA7020 alloy. The results obtained from present mathematical model verify the experimental results. The difference between the results obtained from experimental procedure and the FEA is due to the ignorance of porosity in the matrix and chemical reaction of SiO_2 particles with the constituents of AA7020 alloy.

The normalized elastic modulus is shown in figure 5b. The elastic modulus is normalized with the elastic modulus of AA7020 alloy. The stiffness of the composites increases with increase of volume fraction of SiO_2. The upper limit (UL) values computed by the present mathematical model are higher than those values obtained by the 'Role of Mixtures (ROM)'and FEA. This is because of assumption of voids in the present mathematical model. The shear strength of the composites is low for 30% SiO_2 in the composite (figure 5c). The major Poisson's ration increases with increase of SiO_2 in AA7020 alloy matrix (figure 5d). As seen in figure 6, the matrix fracture and interfacial debonding are found in the composites having 30% SiO_2.

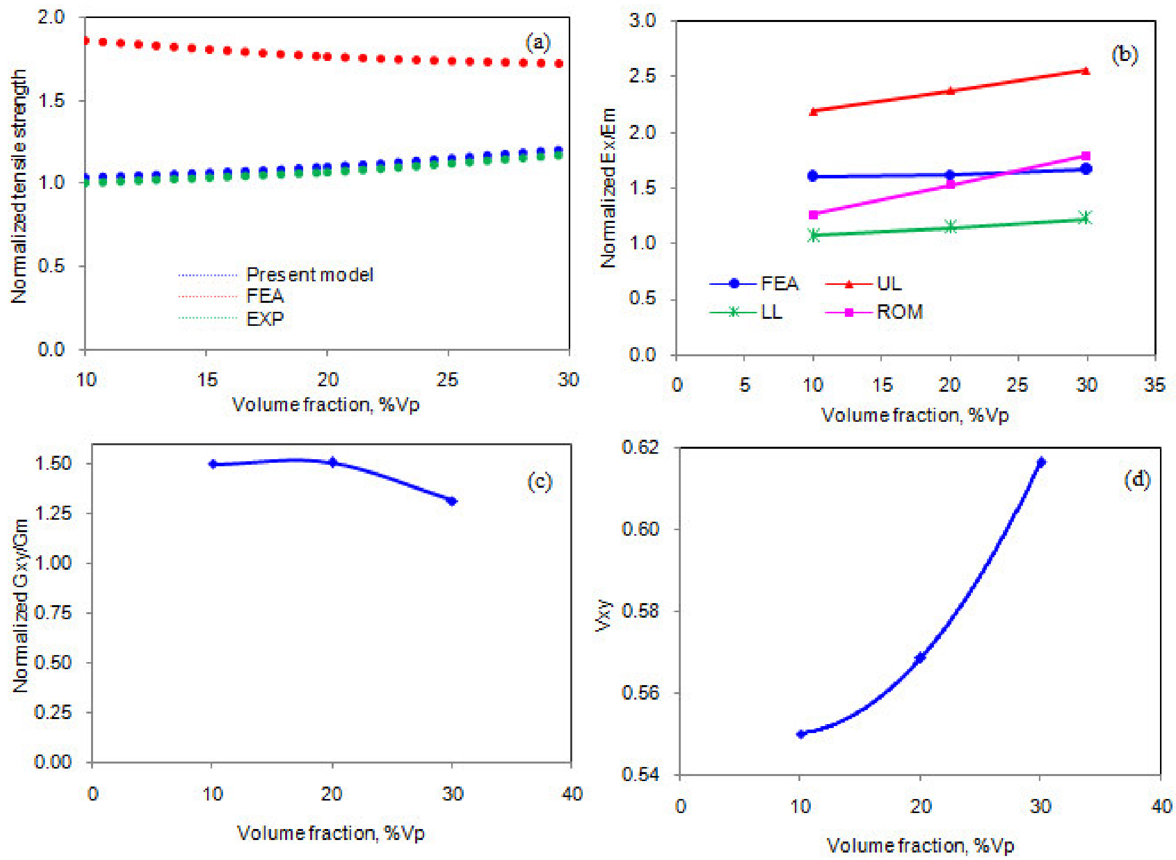

Figure 5: Effect of volume fraction on micromechanical behavior of AA7020/SiO_2 composites.

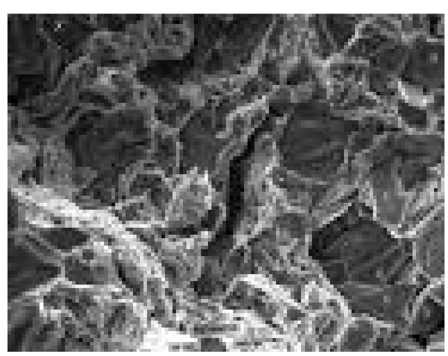

Figure 6: SEM image showing the agglomeration and porosity in AA7020/30%SiO_2 composite.

4.2 Fracture Analysis

If the particle deforms in an elastic manner (according to Hooke's law) then,

$$\tau = \frac{n}{2}\sigma_p \quad (9)$$

where σ_p is the particle stress. If particle fracture occurs when the stress in the particle reaches its ultimate tensile strength, $\sigma_{p,uts}$, then setting the boundary condition at

$$\sigma_p = \sigma_{p,\, uts} \tag{10}$$

The relationship between the strength of the particle and the interfacial shear stress is such that if

$$\sigma_{P,uts} < \frac{2\tau}{n} \tag{11}$$

Then the particle will fracture. From the figure 7b, it is observed that the SiO_2 nanoparticle was not fractured as the condition in Eq. (11) is not satisfied. For the interfacial debonding/yielding to occur, the interfacial shear stress reaches its shear strength:

$$\tau = \tau_{max} \tag{12}$$

For particle/matrix interfacial debonding can occur if the following condition is satisfied:

$$\tau_{max} < \frac{n\sigma_p}{2} \tag{13}$$

It is observed from figure 7a that the interfacial debonding occurs between SiO_2 nanoparticle and AA7020 alloy matrix as the condition in Eq.(13) is satisfied.

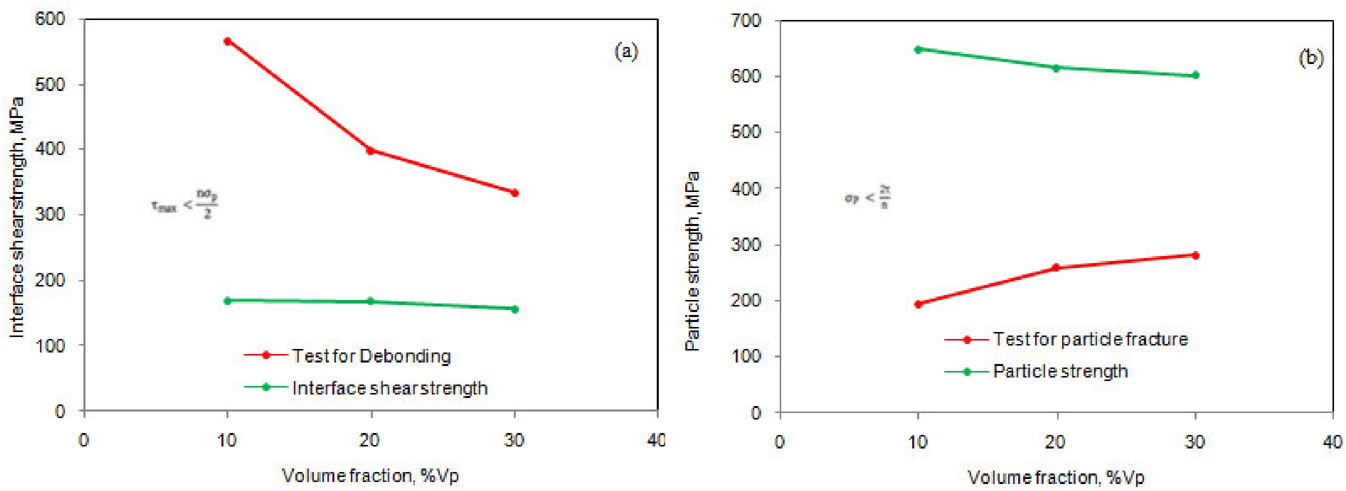

Figure 6: Criterion interfacial debonding (a) and for particle fracture (b).

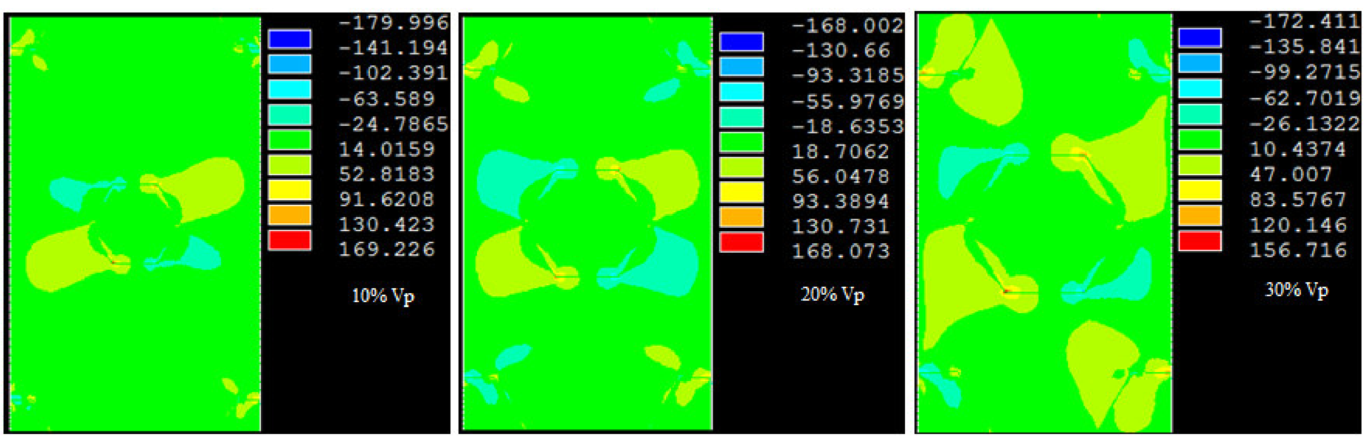

Figure 7: Images of tensile stress obtained from FEA.

As seen from figure 7 the shear stress developed at the interface are higher than that induced in the nanoparticle. Hence, the interfacial debonding was occurred between the particle and the matrix. The matrix fracture is also observed in AA7020/ 30% SiO_2 composites due to high stresses developed in the matrix.

5. CONCLUSION

The microstructure of AA7020 alloy/ SiO_2 reveals the presence of porosity, interfacial debonding and matrix fracture. FEA results are higher than those of experimentation due to ignorance of porosity and chemical reaction during finite element simulation. The shear stress is high at the interface leading to interfacial debonding in AA7020/ SiO_2 composites. Due to lack of load transfer from the matrix to the particle, the fracture in the matrix is also observed.

REFERENCES

1. D. L. Davidson, Fracture characteristics of Al-4pct Mg mechanically alloyed with SiC, Metallurgical Transactions, 18A, 1991, pp. 2115-2138.
2. J. Llorca, P. Poza, Fracture toughness and fracture mechanisms of Al-Al_2O_3composites at cryogenic and elevated temperatures, Material Science and Engineering: A, 206, 1996, pp. 183-193.
3. D. Dunand, A. Mortensen, Reinforced Silver Chloride as a Model Material for the study of Dislocations in Metal Matrix Composites, Material Science and Engineering: A 144. 1991, pp. 179-188.
4. M. Lebyodkin, A. Deschamps, Y. Brechet, Influence of second phase morphology and topology on mechanical and fracture properties if Al-Si alloys, Material Science and Engineering: A, 234, 1997, pp. 481-484.
5. A. Chennakesava Reddy, Assessment of Debonding and Particulate Fracture Occurrences in Circular Silicon Nitride Particulate/AA5050 Alloy Metal Matrix Composites , National Conference on Materials and Manufacturing Processes, Hyderabad, India, 27-28 February 1998, pp. 104-109.
6. B. Kotiveera Chari, A. Chennakesava Reddy, Debonding Microprocess and interfacial strength in ZrC Nanoparticle-Filled AA1100 Alloy Matrix Composites using RVE approach, 2nd National Conference on Materials and Manufacturing Processes, Hyderabad, India, 10-11 March 2000, pp. 104-109.
7. A. Chennakesava Reddy, Local Stress Differential for Particulate Fracture in AA2024/Titanium Carbide Nanoparticulate Metal Matrix Composites, National Conference on Materials and Manufacturing Processes, Hyderabad, India, 27-28 February 1998, pp. 127-131.
8. A. Chennakesava Reddy, Micromechanical Modelling of Interfacial Debonding in AA1100/Graphite Nanoparticulate Reinforced Metal Matrix Composites, 2nd International Conference on Composite Materials and Characterization, Nagpur, India, 9-10 April 1999, pp. 249-253.
9. A. Chennakesava Reddy, Micromechanical and fracture behaviors of Ellipsoidal Graphite Reinforced AA2024 Alloy Matrix Composites, 2nd National Conference on Materials and Manufacturing Processes, Hyderabad, India, 10-11 March 2000, pp. 96-103.
10. S. Sundara Rajan, A. Chennakesava Reddy, Micromechanical Modeling of Interfacial Debonding in Silicon Dioxide/AA3003 Alloy Particle-Reinforced Metal Matrix Composites, 2nd National Conference on Materials and Manufacturing Processes, Hyderabad, India, 10-11 March 2000, pp. 110-115.
11. S. Sundara Rajan, A. Chennakesava Reddy, Role of Volume Fraction of Reinforcement on Interfacial Debonding and Matrix Fracture in Titanium Carbide/AA4015 Alloy Particle-Reinforced Metal Matrix Composites, 2nd National Conference on Materials and Manufacturing Processes, Hyderabad, India, 10-11 March 2000, 116-120.
12. A. Chennakesava Reddy, Cohesive Zone Finite Element Analysis to Envisage Interface Debonding in AA7020/Titanium Oxide Nanoparticulate Metal Matrix Composites, 2nd International Conference on Composite Materials and Characterization, Nagpur, India, 9-10 April 1999, pp. 204-209.
13. A. Chennakesava Reddy, Constitutive Behavior of AA5050/MgO Metal Matrix Composites with Interface Debonding: the Finite Element Method for Uniaxial Tension, 2nd National Conference on Materials and Manufacturing Processes, Hyderabad, India, 10-11 March 2000, pp. 121-127.
14. B. Kotiveera Chari, A. Chennakesava Reddy, Interfacial Debonding of Boron Nitride Nanoparticle Reinforced 6061 Aluminum Alloy Matrix Composites, 2nd National Conference on Materials and Manufacturing Processes, Hyderabad, India, 10-11 March 2000, pp. 128-133.
15. P. M. Jebaraj, A. Chennakesava Reddy, Simulation and Microstructural Characterization of Zirconia/AA7020 Alloy Particle-Reinforced Metal Matrix Composites, 2nd National Conference on Materials and Manufacturing Processes, Hyderabad, India, 10-11 March 2000, pp. 134-140.
16. P. M. Jebaraj, A. Chennakesava Reddy, Continuum Micromechanical modeling for Interfacial Debonding of TiN/AA8090 Alloy Particulate Composites, 2nd National Conference on Materials and Manufacturing Processes, Hyderabad, India, 10-11 March 2000, pp. 141-145.